*J. Fluid Mech.* (2011), *vol.* 672, *pp.* 307–325.  
doi:10.1017/S0022112010006026

# Stability and evolution of uniform-vorticity dipoles

V. G. MAKAROV[1] AND Z. KIZNER[2]†

[1]Interdisciplinary Center of Marine Sciences of the National Polytechnic Institute, La Paz, Baja California Sur 23096, Mexico

[2]Departments of Physics and Mathematics, Bar-Ilan University, Ramat-Gan 52900, Israel

(Received 6 July 2010; revised 9 November 2010; accepted 14 November 2010; first published online 11 February 2011)

Using an iterative algorithm, a family of stationary two-dimensional vortical dipoles is constructed, including translational (symmetric and asymmetric about the translation axis) and orbital (i.e. moving in circles) dipoles. The patches of uniform vorticity comprising a dipole possess symmetry about the axis passing through their centroids and are, generally, unequal in area and absolute value of vorticity. The solutions are discriminated by three parameters, the ratio of the areas of individual vortices, the ratio of their vorticities and the separation between the centroids of the patches. The dipole stability and evolution of unstable states are studied numerically with a contour dynamics method, where the perturbations allowed are, generally, asymmetric. The diagrams of convergence of the iterative algorithm (without any symmetry constraints) are built in three cross-sections of the parameter space: at opposite vorticity of the individual vortices, at equal areas of the vortices and at zero net circulation of the vortex pairs (when inequality of areas of the individual vortices is offset by inequality of the absolute values of vorticity). The convergence bound is shown to be close to the stability bound in the parameter space, and the larger is the separation, the stronger are the perturbations needed to move the dipole out of equilibrium. Typical scenarios of the evolution of unstable symmetric translational dipoles and weakly stable dipoles of other kinds are described, including the transition of a dipole into an oscillating tripole – the scenario that has not been discussed so far.

**Key words:** contour dynamics, vortex breakdown, vortex instability

## 1. Introduction

The first examples of stationary solutions for pairs of symmetric non-overlapping patches of equal or opposite uniform vorticity in two-dimensional ideal-fluid flows were obtained numerically by Deem & Zabusky (1978). Such a vortex pair either rotates steadily at a constant angular velocity around the central point (in the equal-vorticity case), or propagates steadily at a constant translational speed (in the opposite-vorticity case). Shortly thereafter, a more general family of translating dipoles of this type was found by Pierrehumbert (1980), Saffman & Tanveer (1982) and by Wu, Overman II & Zabusky (1984). In fact, the dipoles of this family are symmetric about both the axis of translation and a transverse axis; therefore, we term them *doubly symmetric*.

† Email address for correspondence: zinovyk@mail.biu.ac.il

The next step in this line was taken by Dritschel (1995) who studied pairs of vortex patches of equal or opposite vorticity but, generally, unequal areas and, therefore, of non-zero net circulation. A vortex pair of this type rotates as a whole around some centre that lies either within the line segment connecting the centroids ('centres of mass') of the two patches (in the equal-vorticity case), or outside it (in the opposite-vorticity case). In the latter case, the dipole moves in some circular orbit; this is the reason why we term such solutions stationary *orbital dipoles*. The set of translating doubly symmetric dipoles is a limit case in this category, when the orbit radius goes to infinity. By performing a linear stability analysis, Dritschel (1995) determined the stability properties of his solutions with respect to asymmetric perturbations of the contours bounding the vorticity patches, under the assumption that the perturbations preserve the areas of the patches. He showed that, when the two individual patches constituting a vortex pair are brought sufficiently close to each other, the pair becomes unstable. A similar behaviour was demonstrated in two-layer modons (Kizner, Berson & Khvoles 2002) and in their point-vortex analogues, hetonic quartets (Kizner 2006, 2008).

In this paper, those vortex pairs are considered whose partners can differ not only in area but also in the absolute value of vorticity. Hence, we differentiate the dipoles by three parameters: the ratio of the areas of their individual vortices (or by the relative difference of the areas), the ratio of the vorticity values of the patches (or by the relative difference of these values) and by the relative separation $d$ between the centroids of the vortices. The targets of our research are the following: (i) numerical construction of the broadest possible three-parameter family of stationary dipoles and determination of the convergence domain of our algorithm, (ii) estimation of the stability region in the three-dimensional parameter space for the dipoles found and (iii) studying the typical scenarios of evolution of unstable or slightly perturbed stable dipoles that are close to the stability bound.

Stationary dipole solutions are searched for numerically using an extended version (for a number of uniform-vorticity patches) of an algorithm suggested by Kozlov & Makarov (1998). Although, generally, no symmetry restrictions are imposed, the shapes obtained are always symmetric about the axis passing through the centroids of the two individual vortices. In the special case of doubly symmetric dipoles, the solution is obtained by a mirror-symmetry mapping of a single vortex patch steadily propagating along a rigid straight-line wall.

The dipole stability and evolution of unstable states are studied numerically with a contour dynamics code. In the general case of asymmetric dipoles, the perturbations allowed are also asymmetric. Convergence diagrams for the general algorithm (where no symmetry considerations are invoked) are plotted in three cross-sections of the parameter space: at fixed opposite values of vorticity of the individual vortices, at fixed equal areas of the vortices and at zero net circulation (when inequality of areas of the individual vortices is compensated for by inequality of the absolute values of their vorticity). The convergence domain in the parameter space is given by an inequality $d > d_B$, where $d_B$ is a function of the two remaining parameters. The stability tests run show that all the dipoles obtained with the general algorithm are stable to small asymmetric perturbations, and the larger the $d$, the stronger must be the perturbations to move the dipole out of equilibrium. Special tests performed for the dipoles located on the convergence bound indicate that the latter is close to the stability bound. The stability of doubly symmetric dipoles is considered separately relative to symmetric and asymmetric perturbations; such dipoles are shown to be

stable to symmetric perturbations at any $d$, and to asymmetric perturbations only under the condition that $d > d_B$.

Our contour dynamics simulations reveal two main types of evolution of weakly stable asymmetric dipoles (those located close to the stability bound), and of unstable doubly symmetric dipoles: a dipole, whether translational or orbital, transforms either into a smaller orbital dipole usually accompanied by a relatively small third vortex (this behaviour was observed by Dritschel 1995 in opposite-vorticity dipoles), or into an oscillating tripole. The dipole-to-tripole transition has not been described up to now.

## 2. Definitions and methods

### 2.1. *Basic notions and designations*

We base our consideration on the principle of vorticity conservation in two-dimensional flows of ideal incompressible fluids,

$$\partial\omega/\partial t + u\,\partial\omega/\partial x + v\,\partial\omega/\partial y = 0, \tag{2.1}$$

where $x$ and $y$ are the Cartesian coordinates, $u$ and $v$ are the $x$- and $y$-components of the flow velocity, respectively, and $\omega = \partial v/\partial x - \partial u/\partial y$ is the vorticity.

Consider a dipole vortical structure composed of two simply connected patches in which the non-zero vorticity is concentrated. Within each patch, the vorticity is assumed to be constant and opposite in sign relative to the other patch. Let the areas and vorticity values of the individual patches be, respectively, $S_1$, $S_2$ and $\omega_1 > 0$, $\omega_2 < 0$. Non-dimensional variables are introduced by taking $\sqrt{\bar{S}} = \sqrt{(S_1 + S_2)/2}$ as the linear scale, and by scaling the vorticity with the mean absolute value $\bar{\omega} = (\omega_1 - \omega_2)/2$; accordingly, $1/\bar{\omega}$ serves as the time scale, and $\bar{\omega}$ and $\bar{\omega}\sqrt{\bar{S}}$ as the scales for the angular and linear velocity, respectively. From this point on, all the variables and parameters are regarded as non-dimensional, and symbols $S_1$, $S_2$, $\omega_1$ and $\omega_2$ stand for the non-dimensional areas and vorticities of the patches. Dritschel (1995) used the ratio of the areas occupied by the two vorticity patches to discriminate between different types of dipoles; in a more general situation, this logic suggests the use of the ratio of the absolute values of vorticity in the patches as well. Denoting these ratios as $\alpha$ and $\beta$,

$$\alpha = S_2/S_1, \quad \beta = -\omega_2/\omega_1 > 0, \tag{2.2}$$

we obtain: $S_1 = 2/(1+\alpha)$, $S_2 = 2\alpha/(1+\alpha)$, $\omega_1 = 2/(1+\beta)$ and $\omega_2 = -2\beta/(1+\beta)$.

The coordinates $(x_1^*, y_1^*)$ and $(x_2^*, y_2^*)$ of the centroids (centres of mass) of patches 1 and 2 in the fixed frame of reference $(x, y)$ are given by the following formulas:

$$x_i^* = \frac{1}{S_i}\iint x\,\mathrm{d}x\,\mathrm{d}y, \quad y_i^* = \frac{1}{S_i}\iint y\,\mathrm{d}x\,\mathrm{d}y, \tag{2.3}$$

where $i = 1, 2$, and the integration is performed within patch $i$ only. The distance between the centroids of the two patches,

$$d = \sqrt{(x_1^* - x_2^*)^2 + (y_1^* - y_2^*)^2}, \tag{2.4}$$

will be one of the parameters used to identify a stationary dipole. A consequence of (2.1) is that the net circulation $\Gamma$ and the impulse (linear momentum) components $I_x$ and $I_y$ are constants of motion. They can be written as

$$\Gamma = \iint \omega\,\mathrm{d}x\,\mathrm{d}y = \omega_1 S_1 + \omega_2 S_2 = 4\frac{1-\alpha\beta}{(1+\alpha)(1+\beta)}, \tag{2.5}$$

$$\left.\begin{aligned} I_x &= \iint \omega x \,\mathrm{d}x\,\mathrm{d}y = \omega_1 S_1 x_1^* + \omega_2 S_2 x_2^* = 4\frac{x_1^* - \alpha\beta x_2^*}{(1+\alpha)(1+\beta)}, \\ I_y &= \iint \omega y \,\mathrm{d}x\,\mathrm{d}y = 4\frac{y_1^* - \alpha\beta y_2^*}{(1+\alpha)(1+\beta)}, \end{aligned}\right\} \tag{2.6}$$

where the integrals are calculated over the whole $(x, y)$-plane or, what is the same, within the area occupied by the two vortex patches. The coordinates $x_R$ and $y_R$ of the dipole centroid, which is the centre of the dipole rotation, are

$$x_R = \frac{I_x}{\Gamma} = \frac{x_1^* - \alpha\beta x_2^*}{1-\alpha\beta}, \quad y_R = \frac{I_y}{\Gamma} = \frac{y_1^* - \alpha\beta y_2^*}{1-\alpha\beta}; \tag{2.7}$$

$x_R$ and $y_R$ are also constants of motion. From (2.5) and (2.7), it is immediately seen that the conditions $\alpha\beta = 1$ and $\Gamma = 0$ are equivalent and that the condition $\alpha\beta = 1$ determines translational dipoles, i.e. those whose centres of rotation lie at infinity. At $\alpha\beta \neq 1$, the coordinates of the dipole centroid are finite. In this case, the dipole is orbital, and its centre of rotation lies in the straight line passing through the points $(x_1^*, y_1^*)$ and $(x_2^*, y_2^*)$, but outside the segment connecting these points.

The location of the geometrical centre $(x_g, y_g)$, which appears to be a convenient characteristic to represent the trajectory of the dipole as a whole, depends on the shape, size and mutual arrangement of the patches and not on their vorticities:

$$x_g = \frac{x_1^* + \alpha x_2^*}{1+\alpha}, \quad y_g = \frac{y_1^* + \alpha y_2^*}{1+\alpha}. \tag{2.8}$$

The family of translational dipoles composed of patches having the same areas and opposite vorticities, $\alpha = \beta = 1$, was obtained by Pierrehumbert (1980), while the case of $\beta = 1$ and arbitrary $\alpha$ was investigated by Dritschel (1995). We are considering a family of dipole solutions at arbitrary $\alpha$ and $\beta > 0$. Below, it will be seen that, in the set of stationary dipole configurations that can be obtained with our iterative algorithm, a specific dipole (normalized as described above) can be identified by the three parameters $\alpha$, $\beta$ and $d$. In fact, the visualization of the convergence (or stability) region becomes easier if we change from parameters $\alpha$ and $\beta$ to the relative differences of the areas of the patches and of their vorticities, i.e. to $\delta S = (1-\alpha)/(1+\alpha)$ and $\delta\omega = (1-\beta)/(1+\beta)$, respectively. Therefore, below, each dipole will be identified by the three parameters $\delta S$, $\delta\omega$ and $d$.

### 2.2. *Methods*

The method of contour dynamics was suggested by Zabusky, Hughes & Roberts (1979) for high-resolution simulation of the evolution of uniform-vorticity patches. In more recent times, the method was supplemented with a procedure of reconnection of bounding contours, namely, of cutting off thin vorticity filaments and pooling nearby patches (or filaments) of the same vorticity to create bigger patches; in this modification, the method came to be called the contour surgery method (Dritschel 1988). Various numerical implementations of the method differ from each other in the mode of approximation and surgery of the contours, and in the way of numerical integration and differentiation. Below is a brief description of the algorithm used in this work.

Following Kozlov (1983), we parameterize the coordinates $(\xi, \eta)$ of points belonging to the boundary contour of a simply connected patch of constant vorticity $\omega$ by setting $\xi = \xi(\lambda, t)$ and $\xi = \xi(\lambda, t)$, where $0 \leqslant \lambda \leqslant \Lambda$; the contour is circuited counterclockwise when $\lambda$ varies from 0 to $\Lambda$, and $\xi$ and $\eta$ are periodic functions of $\lambda$ with the period $\Lambda$.

Once the shape and location of the contour are known, the flow induced by the patch is found via the Poisson equation relating the flow streamfunction and the vorticity field. This yields the following formulas for the velocity components of the flow:

$$\left.\begin{aligned} u(x,y,t) &= \frac{\omega}{2\pi}\int_0^{\Lambda}[\eta(\lambda,t)-y]g(\lambda,x,y,t)\,\mathrm{d}\lambda,\\ v(x,y,t) &= -\frac{\omega}{2\pi}\int_0^{\Lambda}[\xi(\lambda,t)-x]g(\lambda,x,y,t)\,\mathrm{d}\lambda, \end{aligned}\right\} \tag{2.9}$$

where

$$g(\lambda,x,y,t)=\frac{\dot\eta[\xi(\lambda,t)-x]-\dot\xi[\eta(\lambda,t)-y]}{[\xi(\lambda,t)-x]^2+[\eta(\lambda,t)-y]^2}, \tag{2.10}$$

and dot denotes differentiation with respect to $\lambda$. The full velocity is a sum of the velocities induced by individual patches. The velocity at which a point $(\xi,\eta)$ on a contour moves is

$$\frac{\mathrm{d}\xi}{\mathrm{d}t}=u(\xi,\eta,t),\quad \frac{\mathrm{d}\eta}{\mathrm{d}t}=v(\xi,\eta,t). \tag{2.11}$$

Equations (2.9)–(2.11) are discretized by distributing a set of nodes in each contour at a distance $\Delta C$ measured along the contour; time is discretized with a step $\Delta t$. By so doing, we arrive at a system of ordinary differential equations (2.11) written for each node. These equations are solved with a fourth-order Runge–Kutta method. To compute the integrals in the right-hand sides of these equations (see (2.9) and (2.10)) and also to estimate the minimal width of each patch and the minimal distance between any pair of contours, at any fixed $t$, the coordinates $\xi(\lambda,t)$ and $\eta(\lambda,t)$ are approximated with a periodic cubic spline. The patches are split (or merged) when the minimal width (or distance) becomes less than $0.2\Delta C$, and the vorticity debris of the area smaller than 0.001 are removed. Thereupon, new nodes are arranged in the contour at the same distance $\Delta C$. For the contour surgery, an original code (Makarov 1991) is used. Along with the general algorithm for vorticity patches on an unbounded plane, a version valid for patches located in a half-plane with a rigid wall is employed to simulate the evolution of a doubly symmetric translational dipole subjected to perturbations symmetric about the translation axis.

At the stage of tuning the contour dynamics code, $\Delta t$ was varied from 0.1 to 0.001 and $\Delta C$ from 0.1 to 0.01. It was found that, at $\Delta t\leqslant 0.0025$ and $\Delta C\leqslant 0.015$, an increase in resolution did not affect the results materially. Therefore below, the combination of $\Delta t=0.0025$ and $\Delta C=0.015$ (the latter corresponds to arranging of 420 nodes over a circle of a unity radius) is referred to as the fine resolution combination. The results related to stability and transitions (§§ 3.2 and 3.3) were obtained with just this resolution.

Capturing the shapes of stationary dipoles is based on the fact that, in a co-moving frame of reference, the total velocity at any point of a contour bounding a vorticity patch should be tangent to the contour. This velocity is a sum of the velocity $(U, V)$ of the incoming flow caused by the motion of the frame, and the velocity $(u, v)$ in a fixed frame of reference (see (2.9) and (2.10)). For a translational dipole, $U$ and $V$ are constants, and for an orbital dipole, $(U, V)$ is the linear velocity of a rigid-body rotation at a constant angular velocity around a fixed centre determined by (2.7). Using the above-described parameterization, the kinematic condition of stationarity can be written as

$$[u(\xi,\eta;\lambda)+U(\xi,\eta;\lambda)]\dot\eta-[v(\xi,\eta;\lambda)+V(\xi,\eta;\lambda)]\dot\xi=0. \tag{2.12}$$

The integro-differential equation obtained by substitution of (2.9) and (2.10) into (2.12) relates the as yet unknown shape of the vorticity patches and the incoming flow. This equation is solved with an iterative procedure, which is an extension to a number of stationary patches of the algorithm employed by Kozlov & Makarov (1998) for capturing the shape of a unique vortex patch in a prescribed exterior flow (see also Makarov & Bulgakov 2008). As in the algorithm of Wu *et al.* (1984), a constraint is imposed on the shape of vorticity patch, according to which any patch must be star-convex. In order to force the procedure to converge to a unique dipole solution with a given triple of parameters $\delta S$, $\delta\omega$ and $d$, during the iterations, we keep unchanged the areas of the two patches and the positions of their centroids in the $(x, y)$-plane by making a homothetic stretching/compression and by shifting the patches at the end of each iteration step. A half-plane version of the algorithm is used to seek doubly symmetric translational dipoles. In most of our computations, we use 1000 nodes and stop the computations when the relative distance between two successive approximations of each contour becomes less than $10^{-13}$.

## 3. Results

### 3.1. *Translating and orbital dipole stationary states*

#### 3.1.1. *Doubly symmetric dipoles*

First (mostly for testing our iterative algorithm), we consider the doubly symmetric translating dipoles (in which $\delta\omega = \delta S = 0$) found earlier by Pierrehumbert (1980). Such solutions can be constructed (i) by exploiting the double symmetry, (ii) using only the symmetry about the translation axis (the $x$-axis) and (iii) without imposing any constraints except for the condition that the patches are star-shaped. Versions (i) and (ii) provide undistinguishable results, and in both cases the iterative procedure converges at $d \geqslant d_S \approx 0.528$, where $d_S$ is the limiting separation corresponding to the Sadovskii (1971) dipole in which the boundaries of the patches have two vertices each and a mutual rectilinear segment at the translation axis. In contrast, the general algorithm (iii) diverges when $d$ is under some critical level $d_0 \approx 0.775$ even if, as the initial guess, we utilize the solution constructed with one of the versions (i) and (ii). At $d > d_0$, the solutions obtained with any one of the three versions of the algorithm coincide to within small discretization errors. In the computations initialized in such a way, the divergence always manifests itself at a certain stage by a sharp increase of the relative difference of the perimeters $\delta P = (P_1 - P_2)/(P_1 + P_2)$. This process is attended by the increase (or decrease) of the angular momentum of the vortex pair. The process of loss of symmetry culminates in stopping of the procedure, when, due to the strong deformation, one of the patches ceases to be star-shaped. Note that the smaller the $d$, the earlier the divergence (figure 1).

#### 3.1.2. *Asymmetric dipoles*

When $\delta\omega$ and/or $\delta S$ differ from zero, there exists a convergence bound $d = d_B(\delta S, \delta\omega)$ in the parameter space $(\delta\omega, \delta S, d)$, such that the iteration process converges at $d \geqslant d_B(\delta S, \delta\omega)$ and diverges at $d < d_B(\delta S, \delta\omega)$; obviously, $d_B(0, 0) = d_0$ (see § 3.1.1). Qualitatively, the divergence occurs in the same way as shown in figure 1: one of the patches elongates and bends and, accordingly, $\delta P$ blows up.

In the solutions obtained at $d \geqslant d_B(\delta S, \delta\omega)$, as the critical value $d_B$ is approached, an increase of steepness can be observed in the changes of the angular momentum, relative perimeter difference $\delta P$, excess energy $E$, the gap between the patches $G$ and the angular (or translational) velocity $\Omega$ (or $U$) of the dipole. The angular momentum

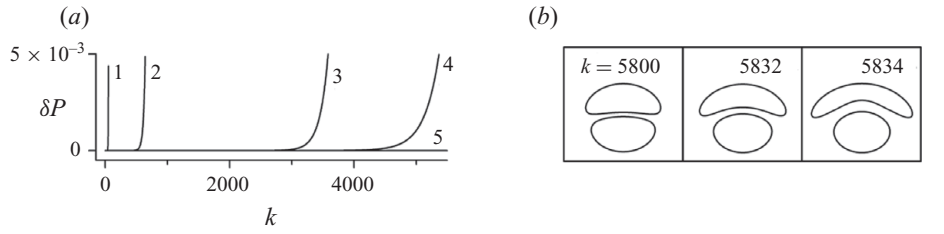


FIGURE 1. Divergence of the general iterative procedure at $d < d_0 \approx 0.775$ and $\delta\omega = \delta S = 0$ (doubly symmetric dipole). (*a*) Relative difference of perimeters $\delta P$ versus the iteration number $k$; the lines labelled 1, 2, 3 and 4 illustrate the divergence at $d = 0.649$, 0.762, 0.773 and 0.774, respectively; line 5, convergence at $d = 0.775$. (*b*) Typical sequence of dipole shapes before the stopping of the iterative procedure, $d = 0.774$.

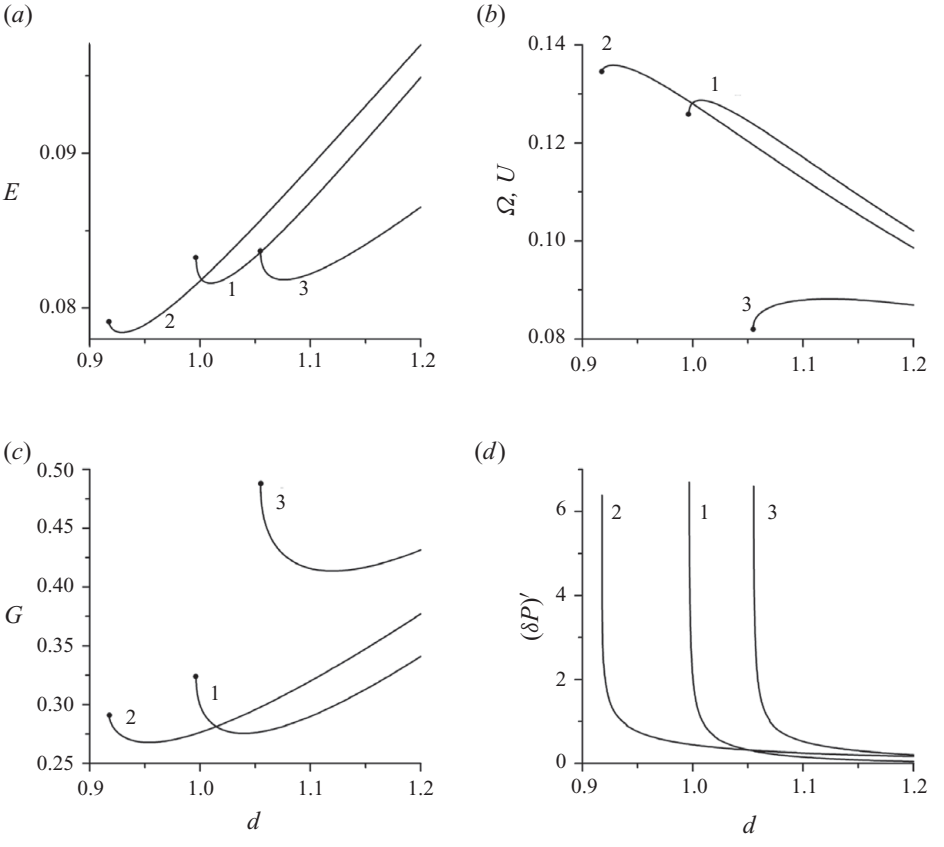


FIGURE 2. Parameters of the asymmetric stationary dipoles as functions of $d$. (*a*) Excess energy $E$; (*b*) angular velocity $\Omega$ (or translational velocity $U$ in the case of $\delta\omega \equiv -\delta S$); (*c*) the gap $G$ between the two patches; (*d*) the derivative $(\delta P)'$ of the relative perimeter difference with respect to $d$. The lines labelled 1 correspond to $\delta\omega = 0$ and $\delta S = 0.5$; labelled 2 to $\delta S = 0$ and $\delta\omega = 0.5$ and labelled 3 to $\delta\omega = -\delta S = 0.5$. Solid circles correspond to $d = d_B$.

and $\delta P$ are monotonic functions of $d$, while each of the parameters $E$, $\Omega$, $U$ and $G$ has an extremum in the vicinity of $d = d_B$. This fact is illustrated by figure 2, where some dipole parameters are plotted for the opposite-vorticity and equal-area orbital dipoles and for asymmetric translational dipoles.

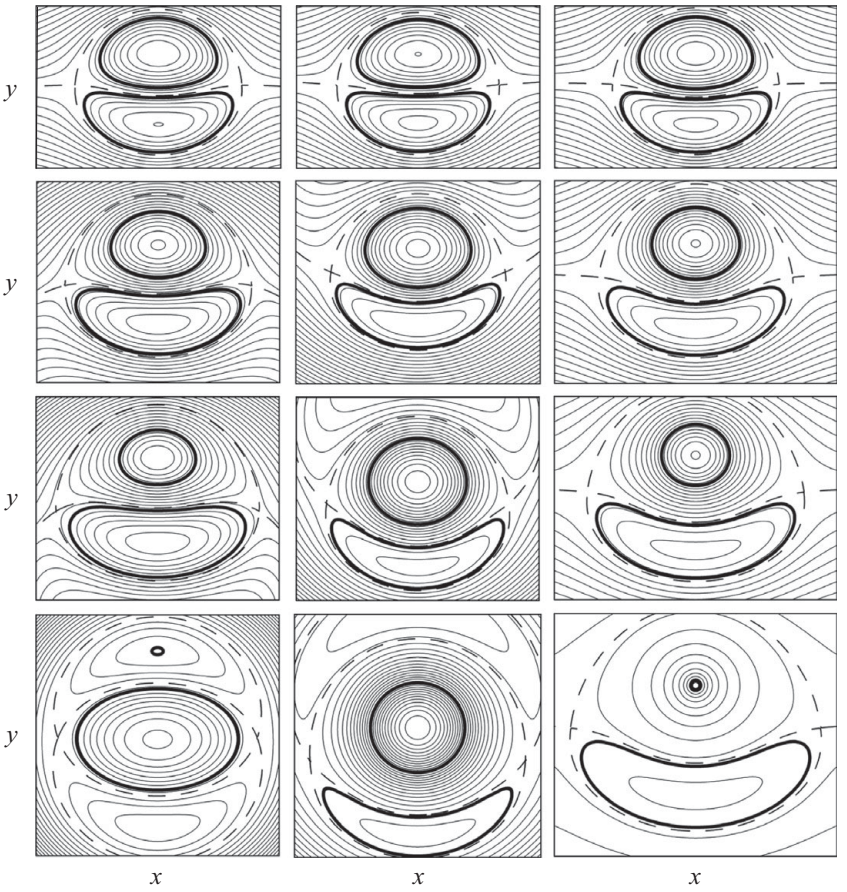


FIGURE 3. Stationary dipoles on the convergence bound $d = d_B(\delta S, \delta\omega)$. Left column, $\delta\omega = 0$ and $\delta S = 0.025$, 0.25, 0.5 and 0.99 (from top to bottom); central column, $\delta S = 0$ and $\delta\omega = 0.025$, 0.25, 0.5 and 0.8 (from top to bottom); right column, $\delta\omega = -\delta S = 0.025$, 0.25, 0.5 and 0.99 (from top to bottom). Bold solid lines, the bounding contours of the vorticity patches; thin solid lines, level contours of the co-moving streamfunction (given at the step of 0.01 in all the plots except for the bottom right-hand one, where the step is 0.001); broken line, the streamfunction separatrix contour.

To identify the solution at fixed $\delta\omega$ and $\delta S$, we use the separation $d$. When $d$ is close to $d_B$, this way of identification is less reliable than at larger $d$ since here small variations of $d$ imply significant variations of other characteristics (figure 2). Therefore, it comes as no surprise that, in the region of high gradients of the dipole characteristics, the iterative algorithm becomes more and more sensitive to numerical errors as $d$ is decreased. This is what leads to the divergence at $d < d_B$. One may even surmise that in terms of $d$, there are, generally, two branches of solutions for which $d = d_B$ is a turning point, and our algorithm captures only one of the two branches (see also § 3.2.2).

Some examples of stationary dipole shapes are shown in figure 3. We confine ourselves to the three cross-sections of the parameter space: $\delta\omega = 0$ (the case of equal absolute values of vorticity considered by Dritschel 1995); the equal-area case $\delta S = 0$, where the patches differ in the absolute values of their vorticity and $\delta\omega = -\delta S$, where the total circulation of the dipole is zero so that a pair of patches of, generally,

unequal areas and absolute values of vorticity propagates steadily (along the $x$-axis). In figure 3, only the dipoles obtained at the convergence bound $d = d_B$ are presented. Obviously, by changing the signs of $\delta\omega$ and/or $\delta S$, dipoles symmetrical to those shown in figure 3 will be obtained.

As $\delta S \to 1$ at $\delta\omega = 0$ or as $\delta\omega \to 1$ at $\delta S = 0$, one of the vortices becomes vanishingly small (figure 3, left column, bottom plot) or the vorticity of one of the patches vanishes (figure 3, mid-column, bottom plot). Because, in both cases, the contribution of one of the vortices in the net circulation (hence, in the induced velocity field) goes to zero, the remaining vortex approaches a shape allowable for a single stationary vorticity patch. In the first case, apparently, the limiting shape of the remaining vortex is an ellipse (the Kirchhoff vortex) while, in the second case, it is a circle. At $\delta S = 0$, we are able to follow the change in shape of the dipole only from $\delta\omega = 0$ up to $\delta\omega \approx 0.8$, because further increase of $\delta\omega$ makes the weak vortex non-star-shaped. In the limit of $\delta\omega = -\delta S \to 1$ (figure 3, right column, bottom plot), the dipole dies out. The case of $\delta\omega = \delta S \neq 0$ is passed over since it is roughly similar to the case of $\delta S = 0$ and $\delta\omega \neq 0$.

### 3.2. *Stability and convergence*

The stability analysis of dipoles is carried out numerically based on short-term contour dynamics simulations, with the above-described stationary dipole solutions taken as initial states. In the special case when the stability of doubly symmetric dipoles to symmetric perturbations is studied, the half-plane version of the algorithm (see § 2.2) should be employed. Certain numerical noise (coming from the discretization and round-off errors) is always present in the computations, leading to disruption of the structure of an unstable dipole. However, in some cases, initial perturbations are deliberately imposed on the stationary states under consideration (see below).

We regard a dipole to be unstable if it responds to small initial and/or repeatedly acting perturbations by considerable changes in the shape and relative positions of the two vorticity patches. In fact, as computations show, if such changes begin, they always lead to a change in the topological structure of the dipole. Of course, any small initial perturbation of the areas occupied by the two patches (even if it does not lead to any structural rearrangements) will necessarily affect the velocity and the trajectory of the dipole as a whole, for example, transforming a translational dipole into an orbital one or changing the orbit radius. However, such kind of response in the absolute motion should not be interpreted as a manifestation of instability, unless the shape of the dipole and its structural integrity are disrupted.

#### 3.2.1. *Doubly symmetric dipoles*

*Asymmetric perturbations.* Doubly symmetric dipoles ($\delta S = \delta\omega = 0$) were scanned in the range $d_S \approx 0.528 \leqslant d < 1.4$ at a small step, and at $d > 1.4$ they were put to the test selectively. Such dipoles proved to be unstable to asymmetric perturbations at $d \leqslant 0.774$ and stable at $d \geqslant 0.775$, which agrees with the stability bound, $d \approx 0.775$, found by Dritschel (1995). Remarkably, this stability bound coincides with the convergence bound $d_0 \approx 0.775$ (see § 3.1.1). The stable and unstable behaviour of dipoles can easily be distinguished when the evolution of the dipole parameters is examined. As an example, in figure 4($a$), the evolution of the relative perimeter difference, $\delta P$, is shown for some values of $d$. The steep, exponential increase/decrease of $\delta P$ (lines 1–3) confirms the instability of dipoles at $d < d_0$, (the sequence of shapes gone through by the dipole at this stage looks similar to that in a divergent iterative process, see figure 1$b$). The stability of dipoles at $d = 0.775$ and $d = 0.776$ is attested by the fact that $\delta P$ remains limited and small (lines 4 and 5) behaving basically in

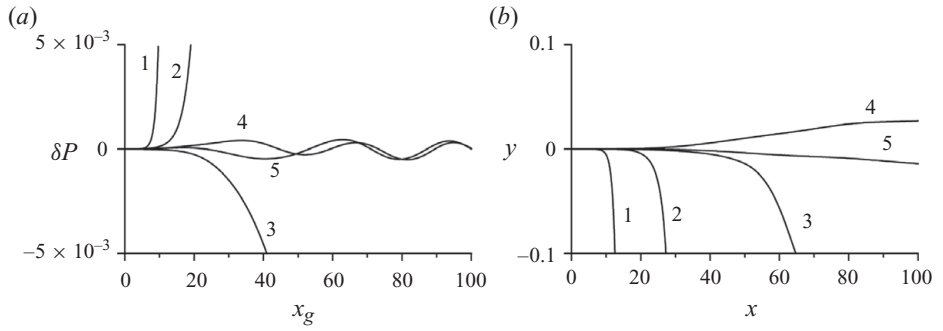


FIGURE 4. Evolution of parameters of doubly symmetric dipoles subjected to asymmetric perturbations. (*a*) Relative perimeter difference $\delta P = (P_1 - P_2)/(P_1 + P_2)$ against the distance $x_g$ travelled by the dipole. (*b*) Trajectory of dipole's geometrical center $(x_g, y_g)$. Lines 1–5 represent the dipoles with the initial $d = 0.649$, 0.762, 0.774, 0.775 and 0.776, respectively (as in figure 1*a*).

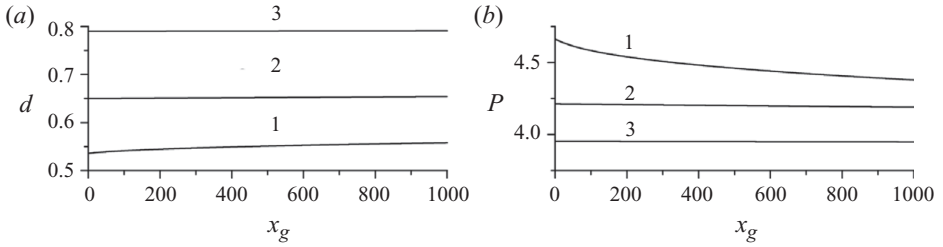


FIGURE 5. Stability of the doubly symmetric dipoles to symmetric perturbations. (*a*) Separation $d$ and (*b*) the single-patch perimeter against the distance travelled by the dipole. Lines 1–3 correspond to the initial $d = 0.536$, 0.65 and 0.79, respectively.

the same manner as most of the other parameters behave. The weak bending of lines 4 and 5 in figure 4(*b*) does not contradict the stability of the corresponding dipoles: stable translational dipoles being subjected to small perturbations can move along slightly curved trajectories (see also below, § 3.2.2).

*Symmetric perturbations.* The stability of doubly symmetric dipoles to symmetric perturbations was tested using the half-plane version of the contour dynamics code, which allows following the evolution of a single vorticity patch that moves along a rigid wall ($x$-axis). Some results of these fine-resolution tests are presented in figure 5.

The doubly symmetric dipoles with $d > d_S \approx 0.528$ prove to be stable to symmetric perturbations: all their characteristics barely change during the simulations (see lines 2 and 3 in figure 5). As for the Sadovskii dipole (at $d = d_S \approx 0.528$) and dipoles with $d$ close to $d_S$, their shapes cannot be resolved at sufficient accuracy in the contour dynamics computations: their contours get smoother and somewhat shorter, while the separation, which should be conserved, increases a little (line 1 in figure 5). Should this be interpreted as unstable behaviour or as a manifestation of adiabatic 'creeping' of a stable dipole over the manifold of stationary solutions? To answer this question, we performed special tests in which the states passed by the evolving dipole were fitted by stationary solutions. These tests indicate that the latter option is more plausible. So we categorize all doubly symmetric dipoles ($d > d_S$) as stable with respect to symmetric perturbations.

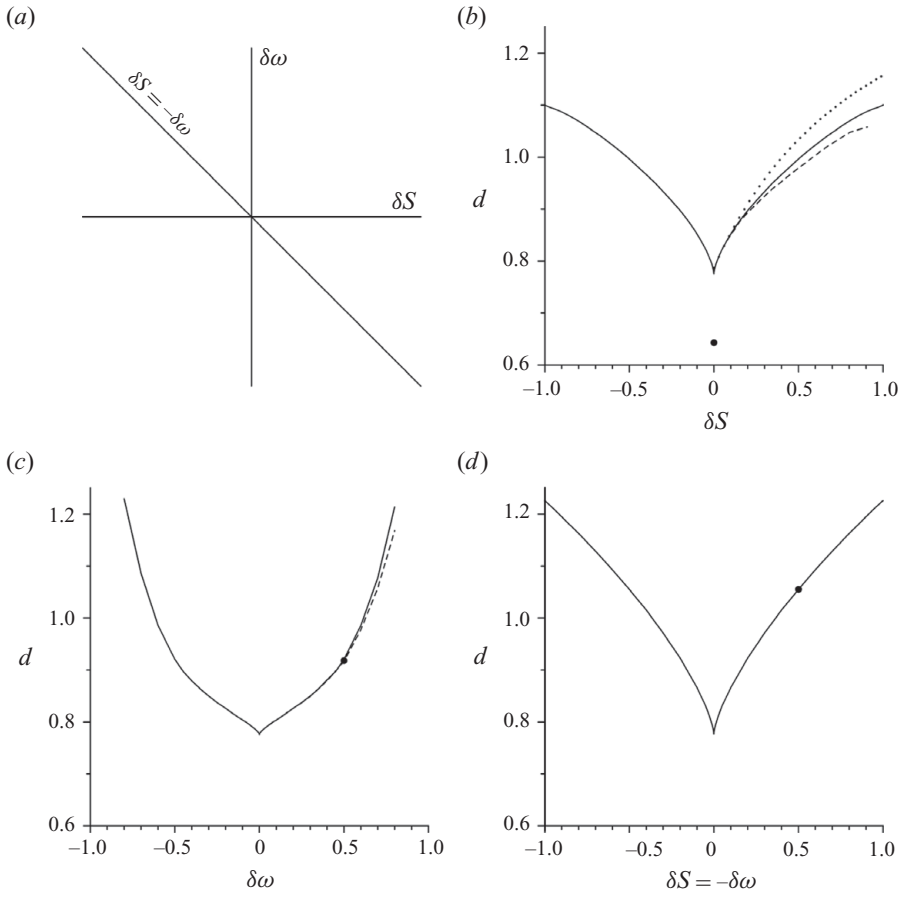


FIGURE 6. Convergence and stability diagrams in three cross-sections of the parameter space. (*a*) Directions of the cross-sections on the $(\delta S, \delta\omega)$-plane. (*b*), (*c*), (*d*) Diagrams at $\delta\omega = 0$ (opposite vorticity), $\delta S = 0$ (equal areas) and $\delta S = -\delta\omega$ (asymmetric translational dipoles), respectively. Solid line indicates the convergence bound above which all dipoles are stable; dashed line, the extremely perturbed separation $d = d_B - \delta d^*$ as a function of $\delta S$ or $\delta\omega$, at which the corresponding dipole begins to behave unstably; in (*d*), the perturbation $\delta d^*$ is under 0.08 % of $d$. Dotted line in (*b*) is the stability bound according to Dritschel (1995). Solid circles symbolize the states whose evolution is discussed in § 3.4.

### 3.2.2. *Asymmetric dipoles*

We proceed now to the stability of orbital and asymmetric translational dipoles (§ 3.1.2). The convergence and stability bounds examined in three cross-sections of the parameter space, at $\delta\omega = 0$, $\delta S = 0$ and $\delta\omega = -\delta S$ (see figure 6*a*), turn out to be close to each other. In figure 6(*b–d*), solid lines indicate the convergence bound $d = d_B(\delta S, \delta\omega)$ above which the iterative procedure for capturing the stationary solutions converges. Each of these cross-sections is obtained based on 30 points distributed regularly over the interval of $0 \leqslant \delta S < 1$ (figure 6*b*), $0 \leqslant \delta\omega \leqslant 0.8$ (figure 6*c*) and $0 \leqslant \delta\omega = -\delta S < 1$ (figure 6*d*); clearly, the cross-sections must be symmetric about the $d$-axis.

An obvious property of the three graphs in figure 6(*b–d*) is the junction of the convergence boundaries in the point $\delta S = 0$, $\delta\omega = 0$ and $d_0 \approx 0.775$. This point demarcates the regions of stability and instability of doubly symmetric dipoles to

asymmetric perturbations and also the regions of convergence and divergence of the general algorithm when applied to the construction of doubly symmetric solutions.

Contour dynamics tests confirm the stability of all the dipoles at $d > d_B(\delta S, \delta\omega)$. As for the dipoles belonging to the convergence bound, in the vicinity of the junction point, the fine-resolution numerical noise is insufficient for causing any visible changes in the dipole shape and behaviour. However, in lower-resolution simulations, these dipoles demonstrate unstable behaviour. As the point representing a dipole in the parameter space is moved along each of the three cross-sections of the convergence bound outward from the junction point, the dipole gradually becomes insensitive to numerical errors.

To estimate the stability threshold of dipoles belonging to the surface $d = d_B(\delta S, \delta\omega)$, an initial perturbation is deliberately introduced by lowering the true separation $d$ by a small value $\delta d$ without changing the shape of the patches. The initially small perturbation $\delta d$ is gradually increased until, at some $\delta d = \delta d^*$, the dipole starts to behave unstably. The onset of instability in a perturbed asymmetric dipole is diagnosed in the same way as in doubly symmetric dipoles (see lines 3 and 4 in figure 4). The results of these tests are provided in figure 6(*b–d*), where in plots (*b*) and (*c*), the broken lines (based on 10 'experimental' points each) represent the extremely perturbed dipole separation, $d = d_B - \delta d^*$ (as a function of $\delta S$ or $\delta\omega$, respectively), at which the unstable behaviour shows up. In the cross-section $\delta S = -\delta\omega$, the perturbations needed to induce unstable behaviour are really small, $\delta d^* < 0.08\,\%$. Thus, in this specific case (figure 6*d*), the stability bound can be identified with the convergence bound.

Notice that at $\delta\omega = 0$, we find stable dipoles below Dritschel's (1995) stability bound (figure 6*b*, dotted line). This can be explained by the fact that, to identify a dipole, we have chosen $d$ (in addition to $\delta\omega$ and $\delta S$) whereas Dritschel uses for this purpose the ratio of the transverse size of the upper (relative to the $x$-axis) vorticity patch to the entire transverse size of the dipole; we denote this ratio as $D$. Of course, it is possible to establish a functional relation between $D$ and $d$. However the data provided by Dritschel (1995) suggest that, at a fixed $\delta S > 0$, the relation $D = D(d)$ is not a one-to-one function but has two branches matching at $d = d_B(\delta S, 0)$. By using our algorithm, we are able to obtain only the solutions lying on the upper branch (see § 3.1.2); these solutions are stable. In contrast, Dritschel achieves the lower-branch dipoles as well. The lower-branch dipoles located close to the turning point are stable, whereas the dipoles distant from this point (and lying on the lower branch) are not. In terms of $d$, this means that the stability bound for the lower-branch dipoles is located on the right of the turning point. This is why, in figure 6(*b*), the line standing for Dritschel's stability bound runs above the line representing the convergence bound of our algorithm (the latter line apparently coincides with or is close to that composed of the turning points).

### 3.3. *Transitions*

Here the results of three long-term simulations are presented. In figure 6(*b–d*), the initial locations in the parameter space of the three dipoles considered below are marked by solid circles. These examples illustrate the typical behaviour of a doubly symmetric dipole ($\delta\omega = \delta S = 0$) which is strongly unstable to asymmetric perturbations, and the transitions made by the dipoles located on the convergence bound at $\delta\omega \neq 0$ and $\delta S = 0$, and at $\delta S = -\delta\omega \neq 0$. In the latter two cases, the dipoles are resistant to the numerical noise present in the fine-resolution model. Therefore,

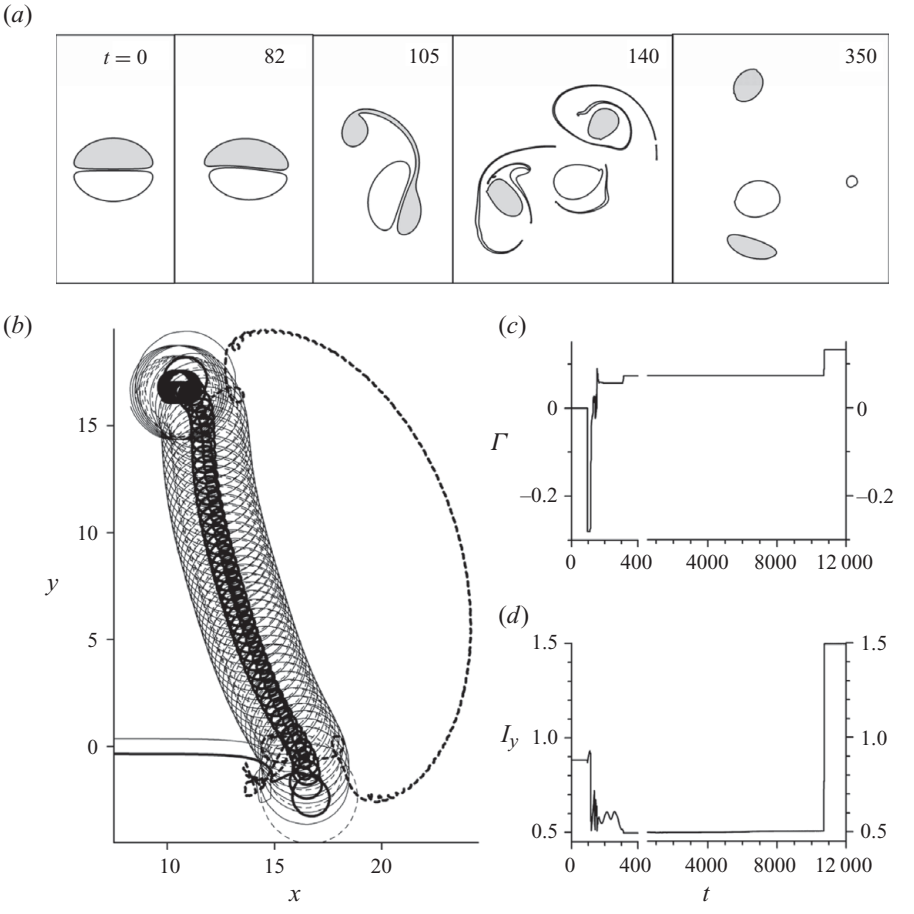


FIGURE 7. The evolution of an initially doubly symmetric dipole with the separation $d = 0.643$. (*a*) The shape of the vorticity patches at $t = 0$, 82, 105, 140 and 350 (from left to right); shaded are the regions of positive vorticity. (*b*) Trajectories of the centroids of the dipole partners before the transition (two almost horizontal lines), and of the tripole core vortex (bold solid line), its two satellite vortices (thin solid and dashed lines) and the small fourth vortex (bold dashed line) – after the transition. (*c*), (*d*) Net circulation $\Gamma$ and the $y$-component $I_y$ of the impulse of the entire ensemble of vortices against time.

to initiate an unstable development, the patches constituting a stationary dipole are brought a little closer to each other.

3.3.1. *Evolution of an unstable doubly symmetric dipole into an oscillating tripole*

The evolution of doubly symmetric dipoles (i.e. where $\delta S = \delta\omega = 0$) unstable to asymmetric perturbations is investigated in the whole segment of their existence, at $d_S \approx 0.528 < d < d_0 \approx 0.775$. One of the two patches always splits into two main parts, and the closer the dipole is to the stability bound $d = d_0$, the more unequal in area are the parts. At $d$ close to $d_0$, this inequality ultimately leads to the emergence of an orbital dipole accompanied by a relatively small remote vortex. If, however, the initial dipole is highly unstable (when $d < 0.67$), the two parts turn out to be comparable in area, and the ultimate state is an asymmetric tripole structure (figure 7*a*) moving in a winding path (figure 7*b*).

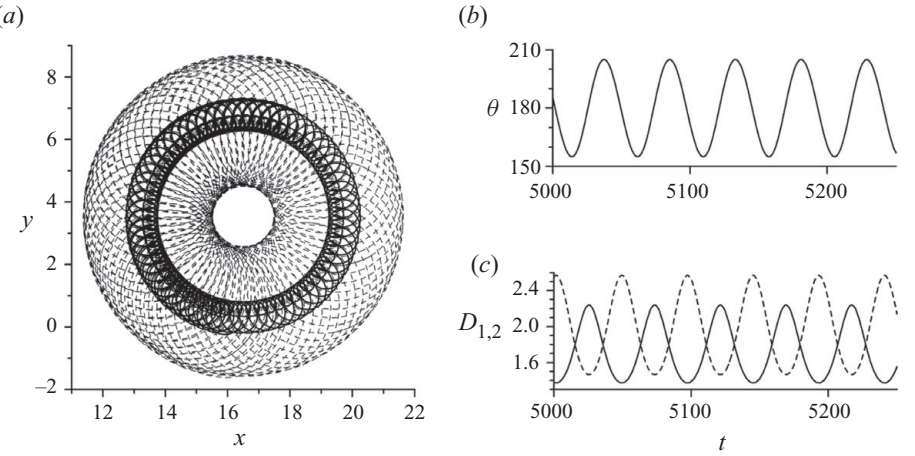


FIGURE 8. The tripole motion after the elimination of the fourth, remote vortex. (*a*) Trajectories of the centroids of the core vortex (bold line) and of one of the satellite vortices (dashed line). (*b*), (*c*) The angle $\theta$ between the line segments drawn from the core centroid to the centroids of the two satellites, and the distances $D_{1,2}$ from the core centroid to the centroids of the satellites against time in a few complete oscillatory cycles.

The motion of a non-equilibrium asymmetric tripole must be a superposition of an intrinsic oscillation, own rotation and translational or orbital motion, depending on whether the net circulation is zero or not (disregarding deformations, debris and filamentation). In the simulation (figure 7) initialized with a doubly symmetric dipole with $d = 0.643$, the net circulation of the entire vortical ensemble – with allowance made for the small negative vortex accompanying the tripole – barely differs from zero (figure 7*c*). This is why, although the circulation of the tripole itself is non-zero, its motion roughly resembles that of an oscillating tripole with zero net circulation (figure 7*b*), until the small fourth vortex collides with the tripole at approximately $t = 11\,000$. Note that significant changes in the invariants may result only from dissipation due to the contour surgery; this effect is especially strong when a transition or collision happens (figure 7*c*,*d*).

We have considered a scenario when, at $t = 400$, all debris and the small fourth vortex have been eliminated from the computations. The results of this simulation for $400 < t < 6000$ are shown in figure 8. The centroids of the three vortices arrange a triangle with periodically varying parameters. As expected, the outer orbit of the tripole is now a circle (figure 8*a*). In addition to the outer orbital motion, the tripole executes its own rotation and undergoes oscillations in the mutual arrangement of the core and the two satellite vortices (figure 8*b*,*c*).

### 3.3.2. *Emergence of a tripole from an equal-area orbital dipole*

Here the transitions will be considered that are made in response to small initial perturbations by equal-area ($\delta S = 0$) dipoles lying on the convergence/stability bound (figure 6*c*). The unstable behaviour begins from some elongation of the weaker-vorticity patch; this is followed by splitting of the patch into two unequal parts and formation of an oscillating tripole configuration. The ultimate configuration depends on the net circulation $\Gamma = 2\delta\omega$ of the initial dipole. The smaller the $\delta\omega$, the closer the initial dipole to the doubly symmetric one (at $d = d_0$) and the more similar its evolution to that described by Dritschel (1995). As $\delta\omega$ is increased, from approximately $\delta\omega = 0.1$, the ultimate three-vortex structure gets more and more compact becoming

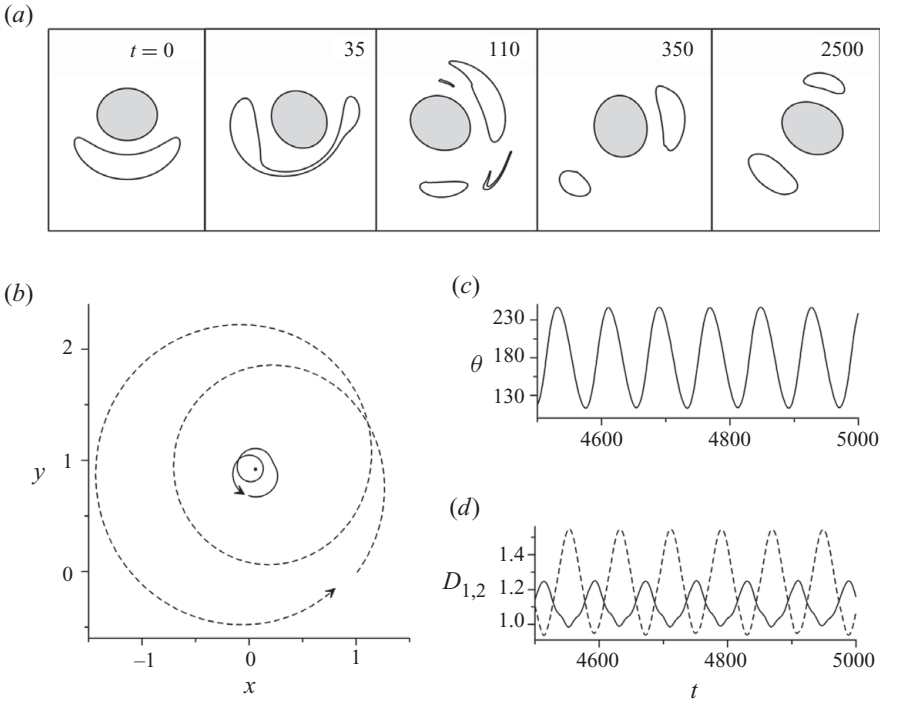


FIGURE 9. Transition of an equal-area orbital dipole ($\delta\omega = 0.5$ and $d = 0.918$) into an oscillating tripole. (*a*) The shape of the vorticity patches at $t = 0$, 35, 110, 350 and 2500. (*b*) Trajectories of the centroids of tripole's core vortex (solid line) and of one of its satellite vortices (dashed line) in one cycle of their oscillations ($t > 4400$); the center of tripole's rotation is marked by a solid circle in the middle. (*c*), (*d*) Same as (*b*) and (*c*) in figure 8.

similar to the oscillating orbital tripole described in § 3.3.1 (figure 8). We note that a tripole emerging from an equal-area dipole has no accompanying vortex that could be at all comparable in size with the tripole itself.

Further increase of $\delta\omega$ leads to strengthening of the core vortex relative to the satellite vortices. Accordingly, the trajectory of the core centroid lies in the vicinity of the rotation centre of the tripole. In figure 9(*a*), the emergence of a tripole from an equal-area dipole with $\delta\omega = 0.5$ (marked by a solid circle in figure 6*c*) is shown; the transition is initiated by decreasing the initial separation $d = 0.918$ by 0.4 %. Notice that the tripole rotation centre and the rotation centre of the original orbital dipole are practically indistinguishable (the solid circle in the middle of figure 9*b*). This is indicative of the fact that very small quantities of vorticity are dissipated by the surgery procedure in this simulation. The periodic, almost elastic character of the intrinsic oscillations of the tripole are evidenced by figure 9(*c*, *d*).

Not always the emerged asymmetric oscillating tripoles survive in long-term simulations. Considerable asymmetry (which happens at sufficiently large $\delta\omega$) can cause so strong oscillations that the satellite vortices eventually approach each other closely and merge. Thereupon, the weak vorticity patch can split again, but in a different proportion, to form an orbital dipole with a third, remote vortex.

### 3.3.3. *Transition of an asymmetric translational dipole into an orbital dipole*

The last issue to be considered in this paper is the non-trivial transition of an asymmetric translational dipole (lying on the convergence/stability bound) into an

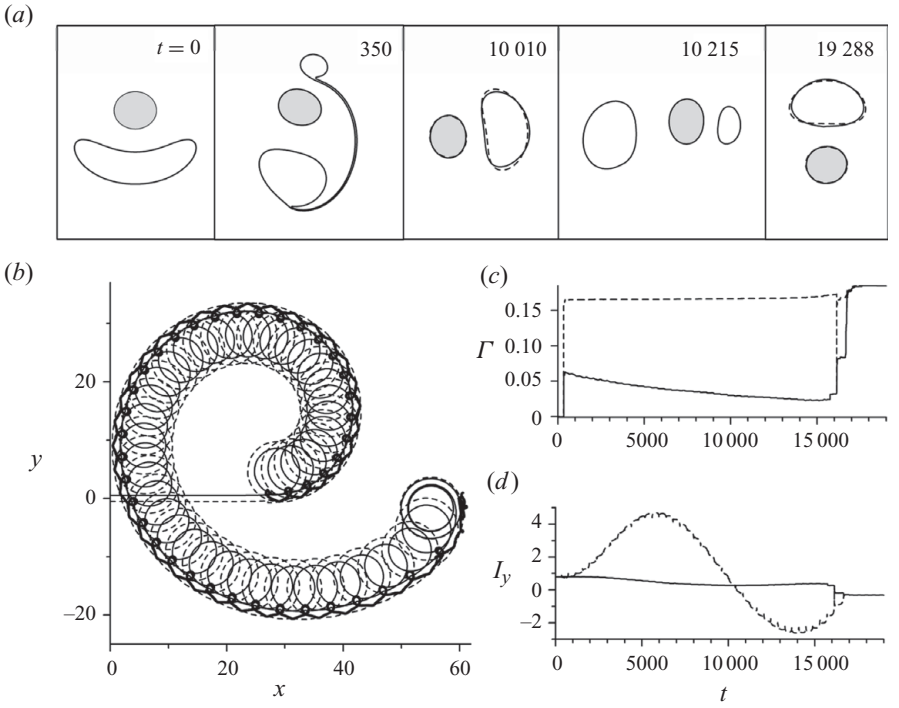


FIGURE 10. Transition of an asymmetric translational dipole with $\delta\omega = -\delta S = 0.5$ and $d = 1.055$ into an orbital dipole. (*a*) The shape of the vorticity patches at $t = 0$, 350, 10 010, 10 215 and 19 288; at $t = 10\,010$, only the dipole without the remote third vortex is shown; dashed lines at $t = 10\,010$ and 19 288 indicate the fitted stationary solutions. (*b*) Trajectories of the centroids of the vortex patches constituting the dipole (solid and dashed lines) and of the third, smaller negative vortex (bold line). (*c*), (*d*) Net circulation $\Gamma$ and the *y*-component $I_y$ of the impulse against time; solid line, the entire ensemble, dashed line, the dipole only.

orbital dipole (figure 10). The initial state shown in the first frame in figure 10(*a*) ($t = 0$) is a dipole with $\delta\omega = -\delta S = 0.5$ and $d = 1.055$, marked by a solid circle in figure 6(*d*). Its unstable evolution is initiated by a reduction of the separation to 1.0549. In the course of the evolution, the negative banana-like patch splits into two unequal parts, but as distinct from the evolution of a weakly unstable doubly symmetric dipole, the smaller part is now comparable in size with the positive patch (figure 10*a*). Therefore, the effect of this smaller vortex on the motion of the orbital dipole assembled by the positive and the bigger of the negative patches becomes significant. Eventually, after a lapse of some 17 000 time units, only the dipole vortex survives (last frame in figure 10*a*).

The intricate shape of the dipole trajectory by $t = 16\,200$ (figure 10*b*) is due to the interaction of the dipole with the third vortex. The dipole itself is quite robust, which is confirmed by the fact that the stationary solution fitted to the dipole at $t = 10\,010$ (the dashed line in figure 10*a*) demonstrates high stability in contour dynamics tests. However, nearly periodically, once within a full turn, the dipole comes within short distance to the third, smaller vortex (figure 10*a*, $t = 10\,215$). This interaction leads to a slow decrease in the net circulation of the entire ensemble (figure 10*c*) and makes the overall motion of the ensemble spirally unwinding (see the trajectory in figure 10*b* and the dashed line in figure 10*d*). The changes in the circulation of the dipole remain

insignificant by approximately $t = 16\,200$ (figure 10*c*). This fact points that, gradually, the dipole slightly weakens, and the third vortex strengthens a little. However, the encounter with the dipole at about $t = 16\,200$ becomes fatal for the smaller vortex: it dissipates via filamentation. The remaining dipole relaxes very fast to an almost stationary orbital dipole with a positive net circulation (figure 10*c*) and the centre of rotation at a fixed point $x \approx 55$, $y \approx 2$ (figure 10*b*). The stationary solution that fits this state (last frame in figure 10*a*, dashed line) is highly stable. Special tests show that, in order to move the dipole out of the equilibrium, its separation $d$ must be diminished by more than 25 % (at fixed $\delta S$ and $\delta\omega$).

## 4. Conclusion

We considered dipolar vortex structures composed of two oppositely-signed uniform vorticity patches. Using an original iterative algorithm, we have constructed a broad family of stationary uniform-vorticity dipoles, both translational and orbital. A translational dipole has zero net circulation and propagates along a straight-line trajectory, while an orbital dipole, having non-zero net circulation, moves in a circular orbit. In an orbital dipole, the areas of the two patches constituting the dipole, or the absolute values of their vorticity are necessarily unequal, the shapes of the two patches being always different from each other.

A stationary dipole, whether translational or rotational, obtained with our algorithm is always symmetric about the axis passing through the centroids of the two patches. A translational dipole can be symmetric about the translation axis if its patches are equal in area and in the absolute value of vorticity; in this case, a dipole is categorized as doubly symmetric. But, in general, a translational dipole is asymmetric about the translation axis.

A properly normalized stationary dipole solution is identified by the relative differences of the areas of the two vorticity patches and of their vorticity, $\delta S$ and $\delta\omega$, and by the separation $d$ between the centroids The solutions belonging to three cross-sections of the parameter space ($\delta S$, $\delta\omega$, $d$) were considered in detail, the cross-sections being: $\delta\omega = 0$ (orbital dipoles with equal absolute values of vorticity in the patches), $\delta S = 0$ (orbital dipoles with equal areas of the patches) and $\delta\omega = -\delta S$ (asymmetric translational dipoles). In these cross-sections, the position of the convergence bound of the general iterative algorithm, $d = d_B(\delta S, \delta\omega)$, was estimated. Stability tests have shown that all dipoles located in the parameter space above this bound are stable with respect to asymmetric perturbations, and the closer the dipole is to the convergence bound, the smaller are the perturbations needed to move the dipole out of equilibrium. These tests indicate that the convergence and stability bounds are close to each other, becoming indistinguishable at sufficiently small $\delta S$ and $\delta\omega$. We have also constructed all the possible doubly symmetric solutions, including those unstable to asymmetric perturbations, and demonstrated their stability to perturbations symmetric about the translation axis.

Particular attention has been given to the typical scenarios of evolution of unstable or slightly perturbed stable dipoles located close to the stability bound. A weakly unstable opposite-vorticity orbital dipole ($\delta\omega = 0$ and $\delta S \neq 0$) makes a transition to a quasi-stationary orbital dipole that weakly interacts with a remote vortex (this case was considered by Dritschel 1995). In a similar way evolves a slightly unstable doubly symmetric dipole ($\delta S = \delta\omega = 0$). If, however, the initial doubly symmetric dipole is highly unstable, the ultimate state is an oscillating tripole accompanied by a small fourth vortex. When all vorticity debris and the small fourth vortex are eliminated, the

remaining tripole moves quite regularly in some circular outer path, while executing intrinsic rotation and periodical oscillations.

An equal-area orbital dipole ($\delta S = 0$, $\delta\omega \neq 0$) lying on the convergence/stability bound also makes a transition either to a dipole or a tripole, depending on the net circulation of the original dipole. The smaller $\delta\omega$ is, the closer is the initial dipole to the doubly symmetric one and, consequently, the more similar is its evolution to the first of the two scenarios outlined above. As $\delta\omega$ is increased, the ultimate three-vortex structure gets more and more compact, becoming similar to the oscillating tripole of the second scenario. Remarkably, in this case, the tripole has no accompanying (fourth) vortex.

A substantially asymmetric translational dipole ($\delta S = -\delta\omega$) lying on the convergence/stability bound makes a transition to an ensemble of an orbital dipole and a smaller third vortex. As distinct from the first scenario, in this case, the effect of the smaller vortex on the motion of the orbital dipole is significant. Although the dipole itself is quite robust, nearly periodically, once within a full turn, the dipole comes within short distance to the third vortex. This interaction makes the motion of the dipole quite intricate.

To sum up, two main results should be highlighted. The first one is the reviled dependence of the dipole stability on the separation between the patches in all kinds of stationary dipoles: larger separation guarantees resistance to stronger perturbations. Such dependence has been observed in baroclinic modons and distributed hetons whose two vorticity 'masses' can overlap (Sokolovskiy & Verron 2000; Kizner *et al.* 2002, Kizner, Berson & Khvoles 2003; Kizner 2006, 2008). Here we have shown that the same is valid for non-overlapping barotropic dipoles. The second result is the discovery of the dipole-to-tripole transition. Whereas the dipole-to-dipole transition had been previously observed in opposite-vorticity dipoles (Dritschel 1995), the observation of the dipole-to-tripole transition appears to be novel. This scenario differs radically from that of the tripole emergence from unstable shielded monopolar vortices (Gent & McWilliams 1986; Carton, Flierl & Polvani 1989; van Heijst & Kloosterziel 1989; van Heijst, Kloosterziel & Williams 1991; Orlandi & van Heijst 1992; Morel & Carton 1994; Makarov 1996; see also Kizner & Khvoles 2004 and references therein).

This research was supported by the National Polytechnic Institute (SIP–IPN projects 20090847 and 20101211) and by the Mexican National System for Researchers (SNI). V.G.M. is indebted to Bar-Ilan University for the financial support for his work visit at BIU. Z.K. acknowledges the support from the Israel Science Foundation grant 628/06. The three anonymous referees are thanked for their helpful comments.

## REFERENCES

Carton, X. J., Flierl, G. R. & Polvani, L. M. 1989 The generation of tripoles from unstable axisymmetric isolated vortex structures. *Europhys. Lett.* **9**, 339–344.

Deem, G. S. & Zabusky, N. J. 1978 Vortex waves: stationary 'V-states', interactions, recurrence and breaking. *Phys. Rev. Lett.* **40**, 859–862.

Dritschel, D. G. 1988 Contour surgery: a topological reconnection scheme for extended contour integrations using contour dynamics. *J. Comput. Phys.* **77**, 240–266.

Dritschel, D. G. 1995 A general theory for two-dimensional vortex interactions. *J. Fluid Mech.* **293**, 269–303.

Gent, P. R. & McWilliams, J. C. 1986 The instability of barotropic circular vortices. *Geophys. Astrophys. Fluid Dyn.* **35**, 209–233.

van Heijst, G. J. F. & Kloosterziel R. C. 1989 Tripolar vortices in a rotating fluid. *Nature* **338**, 369–371.

van Heijst, G. J. F., Kloosterziel, R. C. & Williams, C. V. M. 1991 Laboratory experiments on the tripolar vortex in a rotating fluid. *J. Fluid Mech.* **225**, 301–331.

Kizner, Z. 2006 Stability and transitions of hetonic quartets and baroclinic modons. *Phys. Fluids* **18**, 056601(1–12).

Kizner, Z. 2008 Hetonic quartet: exploring the transitions in baroclinic modons. In *IUTAM Symposium on Hamiltonian Dynamics, Vortex Structures, Turbulence* (ed. A. V. Borisov *et al.*), vol. 6, pp. 125–133. Springer.

Kizner, Z., Berson, D. & Khvoles, R. 2002 Baroclinic modon equilibria on the beta-plane: stability and transitions. *J. Fluid Mech.* **468**, 239–270.

Kizner, Z., Berson, D. & Khvoles, R. 2003 Noncircular baroclinic beta-plane modons: constructing stationary solutions. *J. Fluid Mech.* **489**, 199–228.

Kizner, Z. & Khvoles, R. 2004 The tripole vortex: experimental evidence and explicit solutions. *Phys. Rev.* E **70**, 016307.

Kozlov, V. F. 1983 The method of contour dynamics in model problems of the ocean topographic cyclogenesis. *Izv. Atmos. Ocean. Phys.* **19**, 635–640.

Kozlov, V. F. & Makarov, V. G. 1998 Vortex patch dynamics in a coastal current. *Oceanology* **38**, 456–462.

Makarov, V. G. 1991 Computational algorithm of the contour dynamics method with changeable topology of domains under study. *Model. Mekh.* **5**, 83–95.

Makarov, V. G. 1996 Numerical simulation of the formation of tripolar vortices by the method of contour dynamics. *Izv. Atmos. Ocean. Phys.* **32**, 40–49.

Makarov, V. G. & Bulgakov, S. N. 2008 Regimes of near-wall vortex dynamics in potential flow through gaps. *Phys. Fluids* **20**, 086605(1–11).

Morel, Y. J. & Carton, X. J. 1994 Multipolar vortices in two-dimensional incompressible flows. *J. Fluid Mech.* **267**, 23–51.

Orlandi, P. & van Heijst, G. J. F. 1992 Numerical simulation of tripolar vortices in 2D flows. *Fluid Dyn. Res.* **9**, 179–206.

Pierrehumbert, R. T. 1980 A family of steady, translating vortex pairs with distributed vorticity. *J. Fluid Mech.* **99**, 129–144.

Sadovskii, V. S. 1971 Vortex regions in a potential stream with a jump of Bernoulli's constant at the boundary. *J. Appl. Math. Mech.* **35**, 773–779.

Saffman, P. G. & Tanveer, S. 1982 The touching pair of equal and opposite uniform vortices. *Phys. Fluids* **25**, 1929–1930.

Sokolovskiy, M. A. & Verron, J. 2000 Finite-core hetons: stability and interactions. *J. Fluid Mech.* **423**, 127–154.

Wu, H. M., Overman II, E. A. & Zabusky, N. J. 1984 Steady-state solutions of the Euler equations: rotating and translating V-states with limiting cases. Part I. Numerical algorithms and results. *J. Comput. Phys.* **53**, 42–71.

Zabusky, N. J., Hughes, M. N. & Roberts, K. V. 1979 Contour dynamics for the Euler equations in two-dimensions. *J. Comput. Phys.* **30**, 96–106.